

New photometric investigation of the double ringed galaxy ESO474-G26. Unveiling the formation scenario

M. Spavone^{1,3*}, E. Iodice³, D. Bettoni², G. Galletta¹, P. Mazzei² and V. Reshetnikov^{4,5}

¹*Dipartimento di Fisica e Astronomia, Università di Padova, Vicolo dell'Osservatorio 2, I-35122 Padova, Italy*

²*INAF-Astronomical Observatory of Padova, Vicolo dell'Osservatorio 5, I-35122 Padova, Italy*

³*INAF-Astronomical Observatory of Naples, via Moiariello 16, I-80131 Napoli, Italy*

⁴*St. Petersburg State University, Universitetskii pr. 28, Petrodvoretz, 198504 Russia*

⁵*Isaac Newton Institute of Chile, St Petersburg Branch*

Accepted 2012 July 27. Received 2012 July 23; in original form 2012 June 12

ABSTRACT

We present a detailed photometric study of the peculiar double ringed galaxy ESO474-G26. Near-Infrared (NIR) and optical data have been used, with the main goal to constrain the formation history of ESO474-G26. NIR photometry is fundamental in this kind of study, because gives better constraints on the Spectral Energy Distribution (SED) and well traces the older stellar population of the galaxy. This galaxy presents a very complex structure, with two almost orthogonal rings, one in the equatorial and another in the polar plane, around an elliptical-like object. Due to the peculiar morphology of ESO474-G26, we used both NIR images (J and K bands) to derive accurate analysis of the stellar light distribution, and optical images (in the B, V and R bands) to derive color profiles and color maps to study the structure of the rings. The observational characteristic of ESO474-G26 are typical of galaxies which have experienced some kind of interactions during their evolution. We investigated two alternatives: a merging process and an accretion event.

Key words: Galaxies: photometry – Galaxies: evolution – Galaxies: formation – Galaxies: individual: ESO474-G26 – Galaxies: peculiar – Methods: data analysis.

1 INTRODUCTION

The main aim of the extragalactic astrophysics is to understand how galaxies formed and evolved: the advent of the new all-sky surveys, covering a wide wavelength range, and the high resolution data from the large ground-based and space telescopes have strongly confirmed that gravitational interactions and mergers affect the morphology and dynamics of galaxies from the Local Group to high-redshift universe (Conselice et al. 2003; HDF and HUDF; SDSS). From this kind of studies, there is a growing evidence that mergers play a major role in the formation of early-type galaxies (Ellipticals and S0s), both in the field and in clusters. The traditional debate about the formation of spheroids (Es) and disk (S0s) galaxies, is today re-addressed to understand the origin of slow and fast rotators (see Emsellem et al. 2011 and Khochfar et al. 2011) in which ETGs are today divided. Emsellem et al. (2011) show that about 66% of elliptical galaxies are fast rotators, i.e. they might have a disk component. Tal et al. (2009) found that 73% of nearby ellipticals show morphological feature of interactions.

These observational results support the Cold Dark Matter scenario for galaxy formation (Cole et al. 2000): it is based on the hierarchical mass assembly, where the observed galaxies and their dark halo were formed through repeated mergings of small systems. In this framework, the study of peculiar and interacting galaxies, both at low and at high redshift, has a special role to investigate on the main processes at work during gravitational interactions between galaxies and between galaxies and their environment. In particular, in latest ten years, a big effort has given to study the morphology and kinematics of Polar Ring Galaxies (PRGs) and related objects: in these systems, the existence of two orthogonal components of the angular momentum is a consequence of a “second event” happened in their formation history, thus, PRGs can be considered as the ideal laboratory to study both the gravitational interactions among galaxies and the dark halo shape.

In the PRG catalogue made by Whitmore et al. (1990), the included objects are all classified as polar ring galaxies, where the morphology of central host resemble that of an early-type galaxy (Elliptical or S0) and the polar structure is a ring made up of gas, stars and dust that orbits in a nearly perpendicular plane with respect to central com-

* E-mail: spavone@na.astro.it (MS)

ponent (Schweizer et al. 1983; Bertola et al. 1985). By taking advantage of high resolution spectroscopy and photometry, only subsequent studies on the prototype of PRGs, NGC4650A, have revealed for the first time that the polar structure in this object has the morphology and kinematics of a disk, rather than a ring (see Arnaboldi et al. 1997; Iodice et al. 2002; Gallagher et al. 2002; Swaters & Rubin 2003). From that moment on, by comparing observations and theoretical predictions, studies on polar ring/disk galaxies have tried to address how different kind of interactions (i.e. between galaxies and with environment) let to different galaxy morphologies and kinematics. Currently, in order to account both for the featureless morphology of the central spheroidal galaxy and for the more complex structure of the polar ring/disk, the main formation processes proposed are: *i*) a major dissipative merger; *ii*) tidal accretion of material (gas and/or stars) by outside; *iii*) cold accretion of pristine gas along a filament. In the merging scenario, the PRG results from a “polar” merger of two disk galaxies with unequal mass: the morphology and kinematics of the merger remnants depends on the merging initial orbital parameters and the initial mass ratio of the two galaxies (Bekki 1998a; Bekki 1998b; Bournaud et al. 2005). In the accretion scenario, the polar ring/disk may form by a) the disruption of a dwarf companion galaxy orbiting around an early-type system, or by b) the tidal accretion of gas stripping from a disk galaxy outskirts, captured by an early-type galaxy on a parabolic encounter (Reshetnikov & Sotnikova 1997; Bournaud & Combes 2003; Hancock et al. 2009). The cold accretion scenario has been proposed very recently for the formation of a wide disk-like polar rings: a long-lived polar structure may form through cold gas accretion along a filament, extended for ~ 1 Mpc, into the virialized dark matter halo (Macciò et al. 2006; Brook et al. 2008). In this formation scenario, there is no limits to the mass of the accreted material, thus a very massive polar disk may develop either around a stellar disk or a spheroid. From the “observational” side, as suggested by very recent studies on PRGs (Iodice et al. 2006; Spavone et al. 2010, 2011), the critical physical parameters that allow to discriminate among the three formation scenarios are 1) the total baryonic mass (stars plus gas) observed in the polar structure with respect to that in the central spheroid; 2) the kinematics along both the equatorial and meridian planes; 3) the metallicity and SFR in the polar structure. By studying the chemical abundances in the polar structure of three polar disk galaxies, NGC4650A, UGC7576 and UGC9796, Spavone et al. (2010, 2011) have traced the formation history of these objects by accounting for all the three parameters mentioned above. In particular, the cold accretion scenario was successfully tested for the first time.

In the present paper, we address the formation history of the multiple ring galaxy ESO474-G26, by comparing the observed structure with the predictions from different formation scenarios. Together with the previous one (cited above), this work is part of an ongoing research project which aim to study the morphology, kinematics and SFR of a statistically significant sample of polar ring/disk galaxies and related objects, selected from both the Whitmore’s PRG catalogue and from the new PRG catalogue compiled by Moiseev et al. (2011) based on SDSS data.

1.1 Properties of the PRG ESO474-G26

ESO474-G26 (Figure 1) has been classified as a *possible candidate for polar ring galaxy* (PRC C-3) by Whitmore et al. (1990). This object has a heliocentric radial velocity of $V = 15802 \text{ km s}^{-1}$, which implies a distance of about 211 Mpc, based on $H_0 = 75 \text{ km s}^{-1} \text{ Mpc}^{-1}$, and with this distance $1 \text{ arcsec} \simeq 1 \text{ kpc}$.

This galaxy has two perpendicular and almost irregular rings, one in the equatorial and one in the polar plane, surrounding a central nearly spherical galaxy. Reshetnikov et al. (2005) found very blue optical colors for the rings, typical of late type spirals. Moreover, since both rings rotate around the central galaxy (Whitmore et al. 1990; Reshetnikov et al. 2005), they conclude that ESO474-G26 can be classified as a kinematically confirmed PRG.

Optical spectra also show that the ionized gas rotates with the north and west side receding. Galletta et al. (1997) by analyzing the relatively strong CO signal in ESO474-G26 found that the outer ring (north-south) has the northern side receding, indicating that the molecular gas rotates in the same direction as the ionized one.

The field around ESO474-G26 does not show any object within 10 arcmin or 600 kpc, since the galaxy visible on the NW side is a background object (Galletta et al. 1997).

Reshetnikov et al. (2005) analyzing the luminosity profiles of ESO474-G26 in the optical bands were able to distinguish three components: *i*) the main central body with almost round isophotes ($b/a \sim 0.94$), *ii*) a narrow ring, with a diameter of $\simeq 37'' = 37 \text{ kpc}$, in the equatorial plane, and *iii*) a second (larger) polar ring, with a diameter of $\simeq 58'' = 58 \text{ kpc}$, in the polar plane. Both rings are very irregular.

They also found that the galaxy colors, the ratio of the H_2 mass to blue luminosity and the HI content, correspond to those of an Sb-Sbc spiral, even if the Spectral Energy Distribution (SED) for a prototype advanced merger remnant well fit the observed SED for ESO474-G26. The central galaxy appears to be redder than the galaxy as a whole, but bluer than typical ellipticals, while both rings are bluer than the central body and have colors typical of PRG rings (Reshetnikov et al. 1994, 1995).

The main properties of ESO474-G26 are listed in Table 1.

1.2 Radio emission and star formation rate

In Figure 2 is shown the POSS image of the galaxy with the isocontours of the 1.4 GHz continuum emission from the NRAO VLA Sky Survey (NVSS, Condon et al. 1998) superimposed. The radio emission is elongated in the Northern direction and Condon et al. (1998) reported three sources (the two peaks and the flux in between). If we consider only the emission closest to ESO474-G26 the flux is $F_{1.4} = 4.65 \times 10^{-28} \text{ W m}^{-2} \text{ Hz}^{-1}$ corresponding, with our adopted distance (see Table 1), to a luminosity $L_{1.4} = 2.43 \times 10^{23} \text{ W Hz}^{-1}$. The 1.4 GHz luminosity is insensitive to dust obscuration and for this reason is a good tracer of the star formation rate (SFR_{1.4}). We adopt the calibration of Hopkins et al. (2003) and we found a $\text{SFR} = 130 M_{\odot} \text{ y}^{-1}$ (see Table 2).



Figure 1. Color composite image of ESO474-G26 assembled from images in the B (blue channel), V (green channel) and R (red channel) bands. The north is up, while the east is on the left of the image.

Table 1. Global properties of ESO474-G26.

Parameter	Value	Ref.
Morphological type	Sc peculiar	NED ^a
R.A. (J2000)	00h47m07.5s	NED
Decl. (J2000)	-24d22m14s	NED
Helio. radial velocity	15802 km/s	NED
Redshift	0.052710	NED
Distance	211 Mpc	
Axial ratio	0.65	Reshetnikov et al. (2005)
Absolute magnitude M_B	-22.04	Reshetnikov et al. (2005)
Absolute magnitude M_J	-24.67	This paper
Absolute magnitude M_K	-25.52	This paper
$M(HI)(M_\odot)$	1.7×10^{10}	Reshetnikov et al. (2005)
$M(H_2)(M_\odot)$	2.3×10^{10}	Galletta et al. (1997)
$M(HI)/L_B(M_\odot/L_\odot)$	0.15	Reshetnikov et al. (2005)
$M(H_2)/L_B(M_\odot/L_\odot)$	0.20	Reshetnikov et al. (2005)

^a NASA/IPAC Extragalactic Database

Reshetnikov et al. (2005), converting the far-infrared luminosity to a star formation rate, also found a high rate of star formation ($SFR_{FIR} = 43M_\odot/yr$).

2 OBSERVATION AND DATA REDUCTION

Near-Infrared data - ESO474-G26 belongs to a selected sample of peculiar galaxies observed in the Near-Infrared (NIR) J and K bands in December 2002, with the SofI infrared

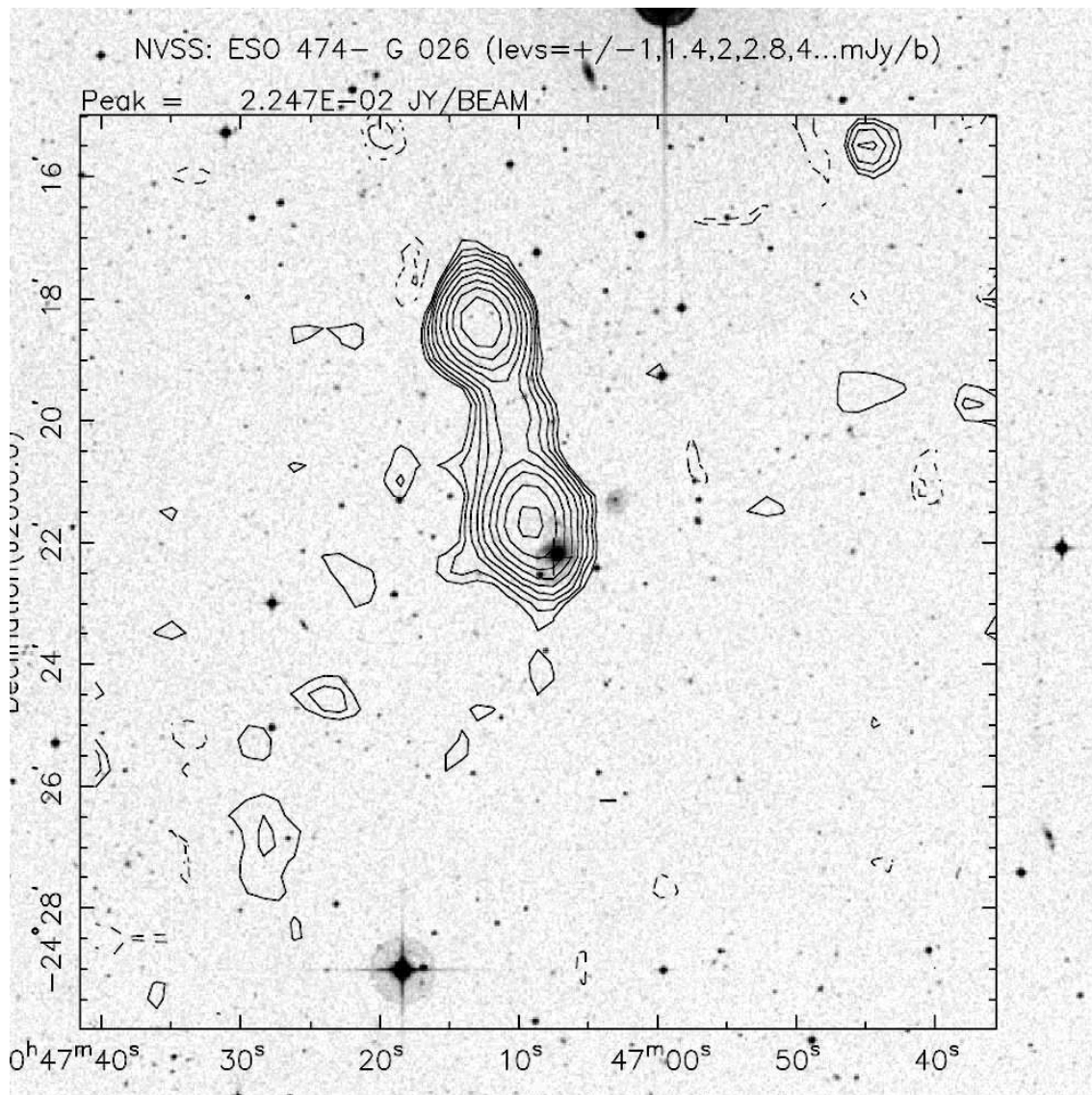


Figure 2. 21 cm contours superimposed to the B band image of ESO474-G26. The north is up, while the east is on the left of the image.

Table 2. Radio fluxes, luminosities and SFRs of the three sources detected by NVSS.

NVSS	RA (J2000)	Dec (J2000)	S1.4 (mJy)	err(mJy)	$L_{1.4}$ (W/Hz)	SFR (M_{\odot}/yr)
004709-242140	00 47 09.06	-24 21 40.4	46.5	2.4	2.4291e+23	1.3e+2
004710-241949	00 47 10.51	-24 19 49.3	9.1	1.3	4.8475e+22	26.8
004712-241823	00 47 12.67	-24 18 23.5	40.9	2.0	2.1787e+23	1.2e+2

camera at the ESO-NTT telescope. The field of view was $4.92 \times 4.92 \text{ arcmin}^2$ with a pixel scale of 0.292 arcsec/pixel. Images were acquired in the offsetting mode: a cycle was defined by several images on the target, interspersed with sky frames and with an integration time of 60 seconds; each object frame was taken with a small offset from the galaxy center and the sky frames were taken before and after each galaxy frame. More cycles were obtained in the K band than in the J band, in order to have a better estimate of the background level. A total exposure time of 360 sec was obtained on the target in the J band and of 1080 sec in the K

band. The average seeing during the observing time is about $\text{FWHM} \simeq 1.1 \text{ arcsec}$.

The data reduction was carried out using the CCDRED package in the IRAF¹ (*Image Reduction and Analysis Facility*) environment. The main strategy adopted for each

¹ IRAF is distributed by the National Optical Astronomy Observatories, which is operated by the Associated Universities for Research in Astronomy, Inc. under cooperative agreement with the National Science Foundation.

data-set included dark subtraction², flatfielding correction, sky subtraction and rejection of bad pixels. Finally, all frames were registered and co-added to form the final science frames.

Several standard stars, from Persson et al. (1998), observed at the beginning, middle and end of each observing night, were used to transform instrumental magnitudes into the standard J and K band systems. The obtained photometric zero points are $Z_P(J) = 23.04 \pm 0.02 \text{ mag/arcsec}^2$ for the J band and $Z_P(K) = 22.35 \pm 0.02 \text{ mag/arcsec}^2$ for the K band.

The calibrated J and K band images of ESO474-G26 are shown in Figure 3. The ring-like structure of the galaxy is still visible in the J band image, while it disappears in the K band one.

Optical data - Photometric observations in the Johnson B, V and Cousins R bands were obtained in August 2002 on the 1.6 m telescope of the Observatorio do Pico dos Dias (operated by the MCT/Laboratorio Nacional de Astrofísica, Brazil), equipped with direct imaging camera and a CCD detector with a pixel scale of 0.18 arcsec/pixel. The average seeing during the observing time is about $\text{FWHM} \simeq 1.3 \text{ arcsec}$. Reduction of the CCD frames was performed as described in Reshetnikov et al. (2005). The photometric calibration was made by using standard stars from the Landolt (1983) and Graham (1982) lists, obtaining the following photometric zero points: $Z_P(B) = 23.29 \pm 0.06 \text{ mag/arcsec}^2$, $Z_P(V) = 23.23 \pm 0.06 \text{ mag/arcsec}^2$ and $Z_P(R) = 23.26 \pm 0.06 \text{ mag/arcsec}^2$, for the B, V and R bands respectively.

3 HOST GALAXY AND RINGS MORPHOLOGY

The NIR images of ESO474-G26 (Figure 3) show that most of the NIR light comes from the host galaxy and its morphology resembles that of an almost round elliptical object. The equatorial ring, with a diameter of about 40 kpc, is within the optical radius of the central galaxy ($\sim 40 \text{ kpc}$), while the polar one has a diameter of about 60 kpc and so it is more extended in radius than the host galaxy. Both rings are more clearly visible in the optical B band image, while they gradually disappear in the J and K bands. However, both NIR and optical images show that the host galaxy is the dominant luminous component, while the rings appear knotty and dusty.

To examine the inner structure of the central host galaxy, and to identify the high frequency residuals with respect to the homogeneous light distribution, we create a residual image produced by taking the ratio of the original reduced image with a smoothed one, where each original pixel value is replaced with the median value in a rectangular window. This has the effect of remove the large-scale structure in the image and emphasize the galaxy substructure. We use the IRAF task FMEDIAN to smooth the original reduced image, by using a two-dimensional window. The window size (7×7) is chosen to best emphasize the inner structure of the central host. The final un-sharp masked im-

age is shown in Figure 4 and it represents the *high frequency residual image* of ESO474-G26.

The most important result obtained by this analysis is the absence of any disk-like structures associated with the host galaxy major axis. The absence of a disk in the host galaxy suggested the use of a Sersic law for the 2D fit of the light distribution in this component (see Sec. 5.1).

4 PHOTOMETRY: LIGHT AND COLOR DISTRIBUTION

The overall morphology of ESO474-G26 is very tricky, due to the presence of two, almost perpendicular, ring-like structures. NIR photometry is necessary to reduce as much as possible the dust absorption that affect the starlight distribution and to accurately analyse it as well as to easily identify the inner structure of ESO474-G26. In addition, optical images are used to derive optical versus NIR color profiles and color maps to study the peculiar structure of this galaxy.

4.1 Isophotal analysis

We used the IRAF-ELLIPSE task on the NIR images to perform the isophotal analysis for ESO474-G26 and the results are shown in Figure 5. The average surface brightness extends up to about 25 and 15 arcsec from the galaxy center for the J and K band respectively; in the K band the half-light radius is $R_e = 9.3 \text{ arcsec}$, while in the J band is $R_e = 10.5$. For a semi-major axis r , in the range $2 \leq r \leq 15 \text{ arcsec}$, the ellipticity and the Position Angle (P.A.) are almost constant and equal to 0.05 and $\sim 40^\circ$, that indicates that in this regions the isophotes are almost round and coaxial. For $0 \leq r \leq 2 \text{ arcsec}$ the ellipticity shows the presence of a flatter structure in the center, with a P.A. of $\sim 80^\circ$ and a twisting of the isophotes of about 50 degrees. For $r \geq 15$ the profiles for the J band result perturbed by the presence of the rings. The shape parameters (Figure 6) are all consistent with zero, thus the isophotes do not significantly deviate from purely elliptical shape.

Figure 7 shows that the radial surface brightness between $1''$ and $10''$ is well reproduced by a de Vaucouleur profile, while in the outer regions we observe a bump, in both J and K profiles, which reflect the presence of the ring-like structures and clearly stands out also in the light profiles (see Figure 15).

In Table 3 we give the total integrated magnitudes within two circular apertures, derived for the NIR J and K bands. The apertures were chosen in order to make easier the comparison with the magnitudes of 2MASS data.

4.2 Color distribution and integrated magnitudes

We have derived the mean J-K color profile (Figure 8), and B-K (Figure 9, left panel) color profiles along both photometric axes of ESO474-G26, and the 2-dimensional B-K color map (Figure 9 right panel). On average, the central regions of the galaxy have redder colors, with a maximum value of J-K $\sim 1.14 \pm 0.04$ and B-K $\sim 4.50 \pm 0.08$. As already showed by the un-sharp masked image, also in the 2D B-K color map we find no trace of a disk-like structure.

We also derived the integrated magnitudes and J-K and

² Bias frame is included in the Dark frame.

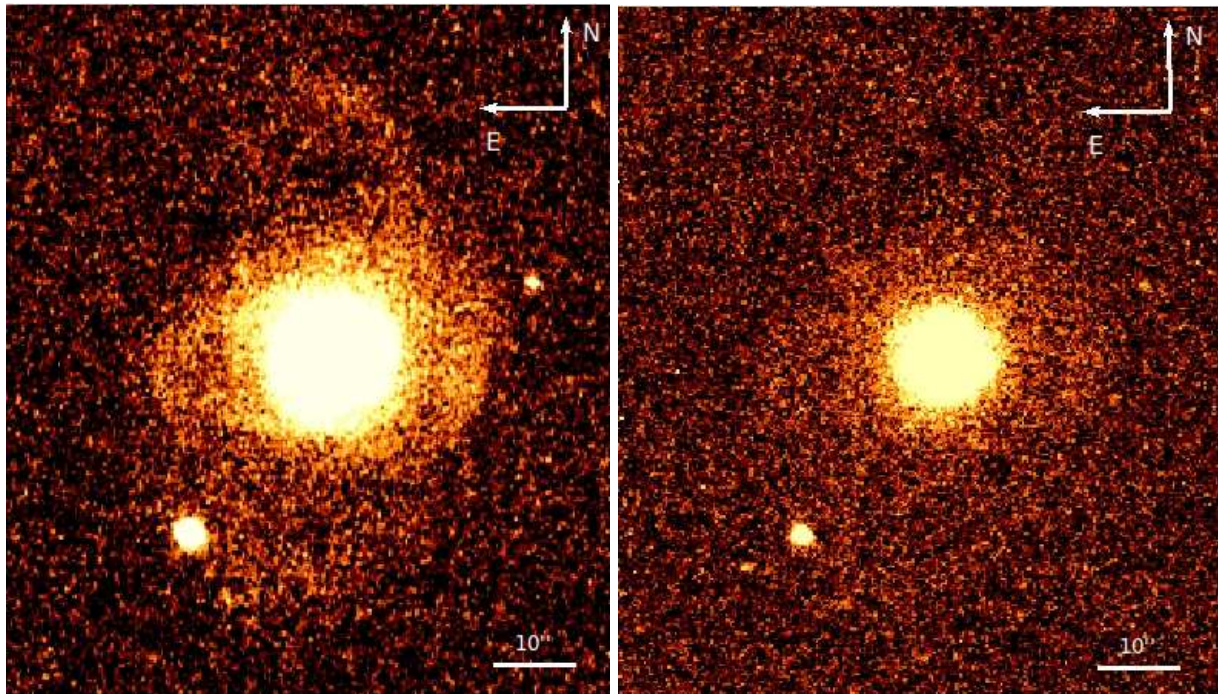


Figure 3. *Left panel*-J-band image of ESO474-G26. *Right panel*-K-band image of ESO474-G26.

Table 3. Magnitudes for ESO474-G26 in circular apertures.

Aperture radius (arcsec)	m_J ± 0.02	m_K ± 0.02	$m_J(2MASS)$ - ^a	$m_K(2MASS)$ -
14.7	12.16	11.10	12.40	11.30
24.0	11.95	-	12.23	11.16

^a The errors on 2MASS magnitudes are 0.01, for both J and K, for the 14 arcsec aperture, and 0.02 and 0.04, respectively for J and K, for the 24 arcsec aperture.

B-K colors in 5 rectangles, as shown in Figure 10: one including the central region of ESO474-G26 and 4 including different regions of the rings. The rectangles are determined from the B band image, using the IRAF task POLYMARK, and used for all bands after the images were registered and scaled. The integrated magnitudes inside each rectangle are evaluated using the IRAF task POLYPHOT.

The derived magnitudes and colors are reported in Table 4.

5 USING COLORS TO DATE THE STELLAR POPULATION

We analyze the integrated colors (optical vs NIR) derived for the rings and spheroid in ESO474-G26 in order to date the average stellar populations of these main components. Taking into account that the integrated colors are the result of both old and young stellar populations, by studying them one can only obtain an indication on how much one is more prominent than the other in the two galaxy components, i.e. Host Galaxy (HG) and rings. As a consequence,

the age estimate is the average value relative to all stellar populations present, which is strongly biased by the last burst of star formation. In the case of ESO474-G26, the central spheroidal component dominates the light in the NIR bands, particularly in the Ks band, while the rings emission becomes weaker from J to Ks bands: this strongly suggests that most of the light relative to an old and evolved stellar population comes from the central HG and in the rings a stellar population as old as that in the HG is absent.

The integrated colors derived for ESO474-G26 are compared with those of PRGs in the sample of Iodice et al. (2002a,b), in order to check whether there are differences in colors and average stellar population age estimates between the main components of this galaxy and other polar rings/disks, which could give some hints on the formation mechanism. As explained in the previous studies on PRGs (Iodice et al. 2002a,b), the B-K versus J-K diagram is used to break the age-metallicity degeneracy; the J-K color is a good estimate of the metallicity and it is quite insensitive to the presence of a young stellar population.

The stellar population synthesis model by

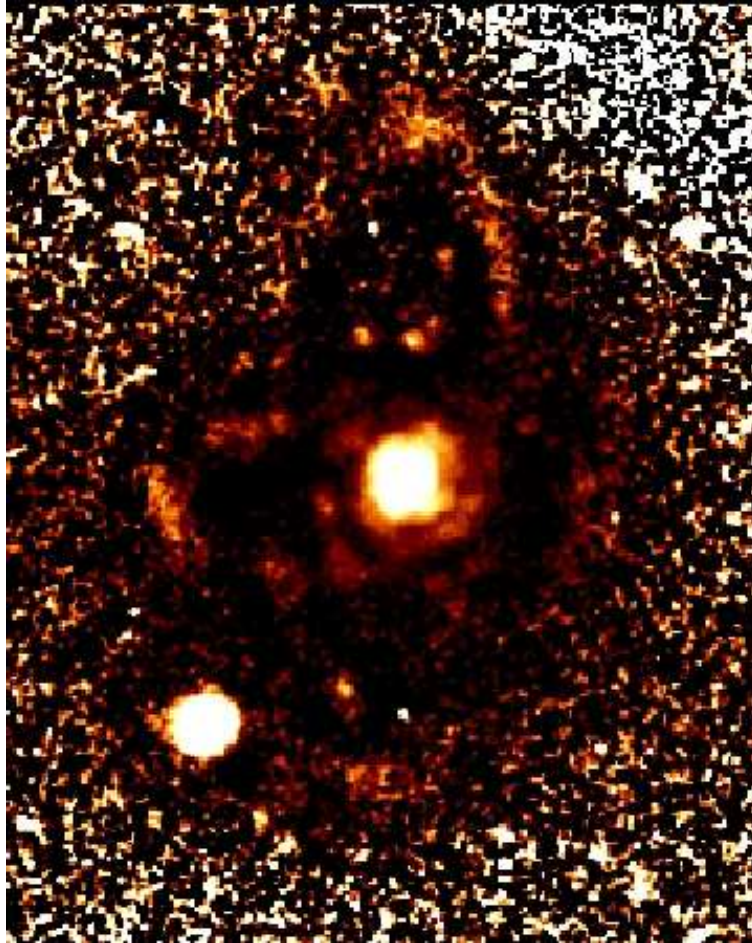


Figure 4. High frequency residual B band image for ESO474-G26. Lighter colors correspond to brighter features. The image size is $90'' \times 115''$, and the north is up while the east is on the left.

Table 4. Integrated and absolute magnitudes and colors of different regions of ESO474-G26.

Component	Region	$m_B(mag)$ ± 0.06	$m_J(mag)$ ± 0.02	$m_K(mag)$ ± 0.02	M_B	M_J	M_K	B-K ± 0.08	J-K ± 0.04
HG	center	13.94	12.51	11.39	-22.68	-24.11	-25.23	2.55	1.12
PR	W	15.30	14.09	13.27	-	-	-	2.03	0.82
PR	E	16.67	15.24	14.78	-	-	-	1.89	0.46
PR	N	15.50	14.16	13.39	-	-	-	2.11	0.77
PR	S	16.97	15.45	14.99	-	-	-	1.98	0.46

Bruzual & Charlot (2003) were used to reproduce the integrated colors in the selected regions, in order to derive an estimate of the average (i.e. old plus the new bursts) stellar population ages in the central component and in the ring-like structures. We selected a set of models that were able to reproduce the average integrated colors observed for the main components of ESO474-G26.

The key input parameters for GISEL (*Galaxies Isochrone Synthesis Spectral Evolution Library*, Bruzual & Charlot 2003) are the Initial Mass Function (IMF), the Star Formation Rate (SFR) and the metallicity. For the central galaxy we adopted a star formation history with an exponentially decreasing rate, that produces a reasonable fit of the photometric properties of

early-type galaxies in the local Universe. It has the following analytical expression: $SFR(t) = 1/\tau \exp(-t/\tau)$, where the τ parameter quantifies the “time scale” when the star formation was most efficient. Adopting $\tau = 1$ Gyr and $\tau = 7$ Gyr, the correspondent evolutionary tracks were derived for different metallicities ($Z=0.1$, $Z=0.02$, $Z=0.05$, $Z=0.008$ and $Z=0.0004$), which were assumed constant with age. For the ring-like structures of ESO474-G26 instead, since they have bluer colors than the host galaxy, which suggests even a younger age for this component, we used models with constant SFR computed for the same metallicities as above, because these models reproduce the integrated colors of local spiral galaxies, in which star formation is still active. In every model it has been assumed that stars

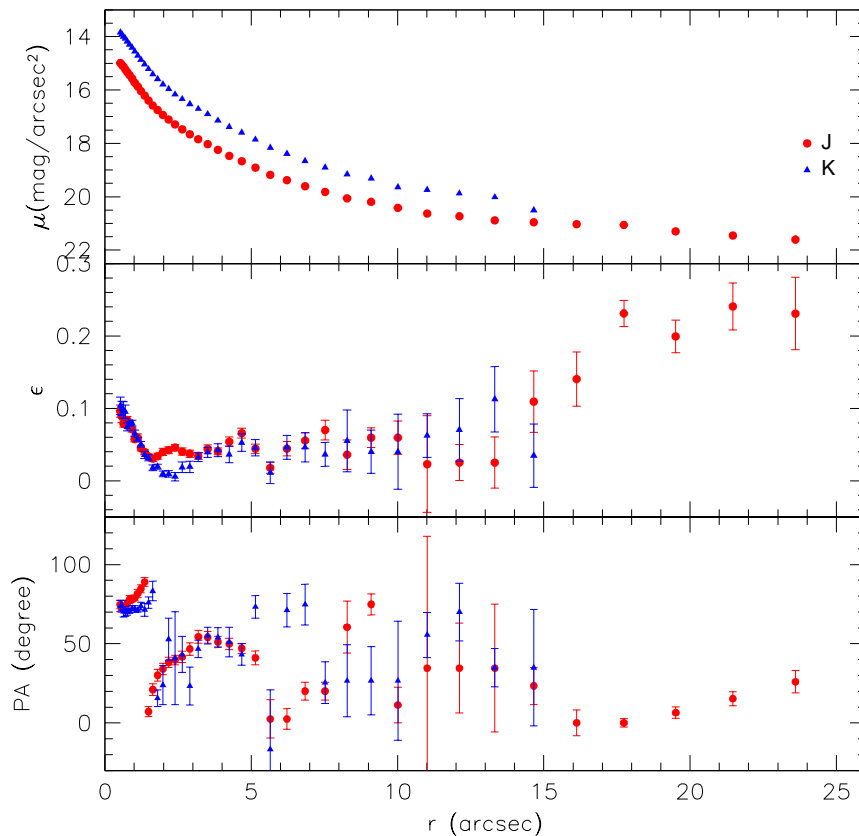


Figure 5. Position Angle (P.A.), Ellipticity (ϵ) and mean surface brightness profile in the J and K bands. The error bar for the surface brightness profile (± 0.02) is within the dimensions of data points.

form according to the Salpeter (1955) IMF, in the range from 0.1 to $125 M_{\odot}$.

Figure 11 shows that the central galaxy is bluer in B-K color than the average values for PRGs in the sample of Iodice et al. (2002a,b), so a younger average age is to be expected, while figure 12 shows that the rings are bluer than the central galaxy. The colors of the NW component are on comparable with other narrow PRGs and not with NGC4650A, which is a wide polar disk, while the SE side appear redder in J-K color (see Table 4), but this could be the effect of a contamination due to the presence of a very bright star in this direction; for this reason the colors corresponding to the South and East side of the rings are not reliable, and so they are not reported in Figure 12. To account for the B-K and J-K colors the best model is that obtained for $Z = 0.1$ for the central galaxy and $Z = 0.05$ for the North and West side of rings, from which we derived an average age, of less than 1 Gyr for the inner region and of less than 0.03 Gyrs for the outer ones. Such values for ages and metallicity turn to be comparable with those derived for the narrow PRGs in the sample of Iodice et al. (2002a,b). This metallicity values are inside the range observed for early type galaxies ($Z_4 \leq Z \leq Z_1$, Bothun & Gregg 1990), but they are higher with respect to the average value, which is around Z_2 . Furthermore, the J-K color for ESO474-G26 (and also for other PRGs) are also consistent with the J-K colors

derived by Rossa et al. (2007) for the interacting galaxies at an intermediate merger stage ($0.5 \leq J - K \leq 1.5$): such range in Figures 11 and 12 correspond to metallicities between Z_3 and Z_2 .

We will show in section 6 that, for both HG and rings, the average ages derived by the integrated colors are comparable with the epoch of formation for these galaxy components estimated by simulations.

5.1 2-Dimensional model of the host galaxy light distribution

Two-dimensional model. We performed a 2-dimensional model of the light distribution of the host galaxy in the Ks and in the B bands. To this aim, we used the GALFIT task Peng et al. (2002) and the resulting structural parameters are listed in Table 5. The Ks image is used to better constrain the structure of the central spheroidal component, since it dominates the light in this band and the emission from the rings and the dust absorption are very weak (see Table 5). The best model for this component is obtained by fitting the galaxy light through a single Sersic law (Sersic 1968). The result is shown in Figure 13: except for the center, where the residuals show the effect of the seeing, there are no evident features, only a diffuse low-luminosity emis-

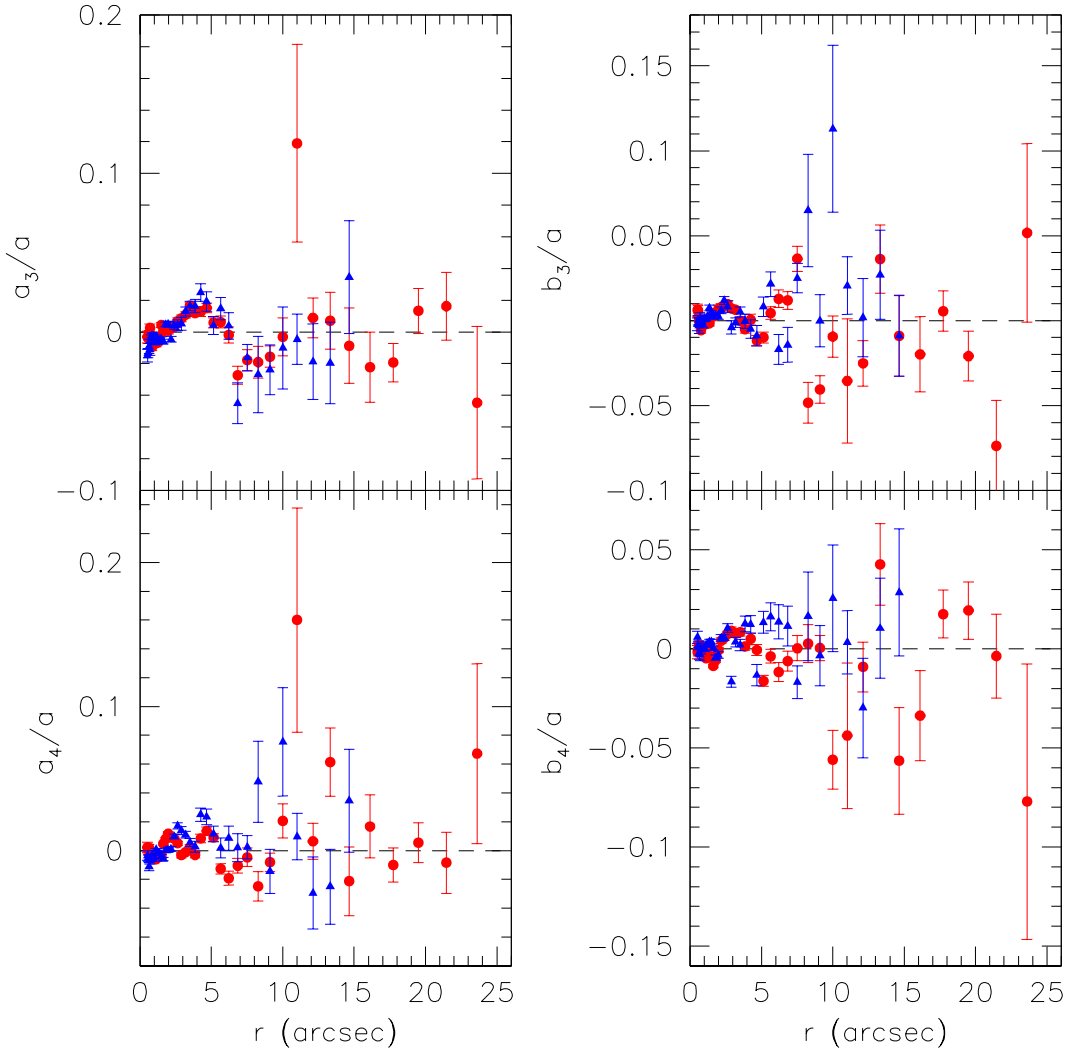


Figure 6. Shape parameters in the J and K bands.

sion is detectable in the North and SE directions, which is the weak residual light coming from the rings.

In order to analyze the complex ring-like structure in ESO474-G26, which is very luminous in the B band, we have also derived the 2D model in this band. By taking into account the constraints for the central galaxy obtained by the 2D model in the Ks band and by accurately mask all the ring structures (which need to be excluded by the fit), the best 2D model in the B band is shown in Figure 14. The residuals appear very different from those in the Ks band: the whole structures of both polar and equatorial rings stands out very clear. Furthermore, it is evident another ring-like structure in the very central regions: it approaches to the galaxy center in the SW quadrant, it extends in the SE tracing a parabolic shape which seems to be connected with the Northern arm of the polar ring.

The comparison between the observed and fitted light profiles along the galaxy major and minor axis (P.A.=0 and P.A.=90 degrees, respectively) is shown in Figure 15 and in

Figure 16, for Ks and B band respectively. In all the profiles and at both position angles, the “additional” light coming from the rings is evident at about 10 arcsec from the galaxy center in the Ks band, and it is much more luminous and extended in the B band, from 10 to 20 arcsec. Except for these regions, inside 10 arcsec, residuals are better than 0.2 mag. In the outer regions ($r \geq 15$ arcsec in the Ks band and $r \geq 35$ arcsec in the B band) light is dominated by background fluctuations.

6 COMPARING THE DATA WITH MODELS

To address the question on the formation scenario for ESO 474-G26 we attempt to best fit its overall SEDs and global properties, analyzing a large set of SPH simulations.

Our SPH simulations of galaxy formation and evolution start from the same initial conditions described in Mazzei & Curir (2003) (MC03 hereafter) and Mazzei (2003)

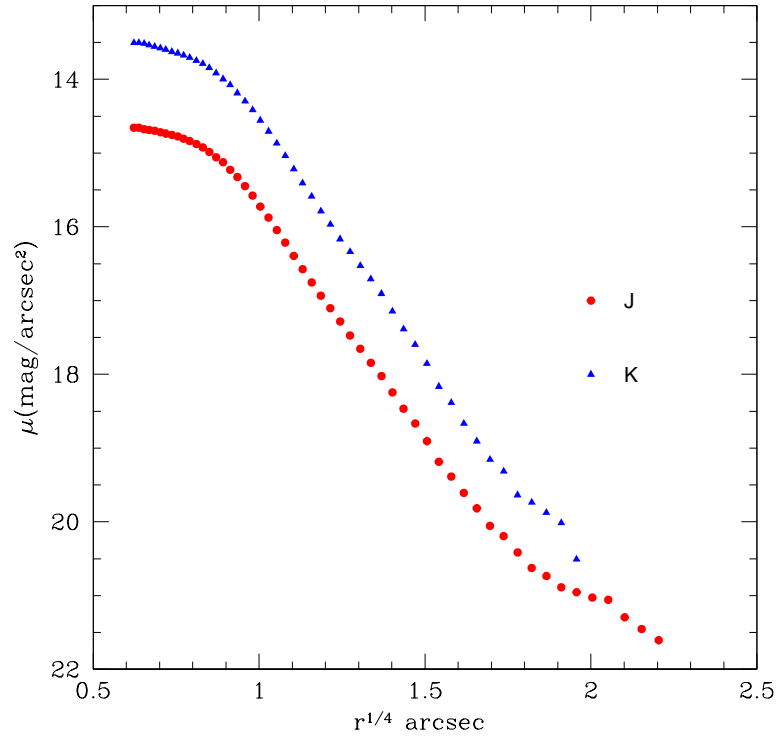


Figure 7. de Vaucouleur radial surface brightness profile. The error bar (± 0.02) is within the dimensions of data points.

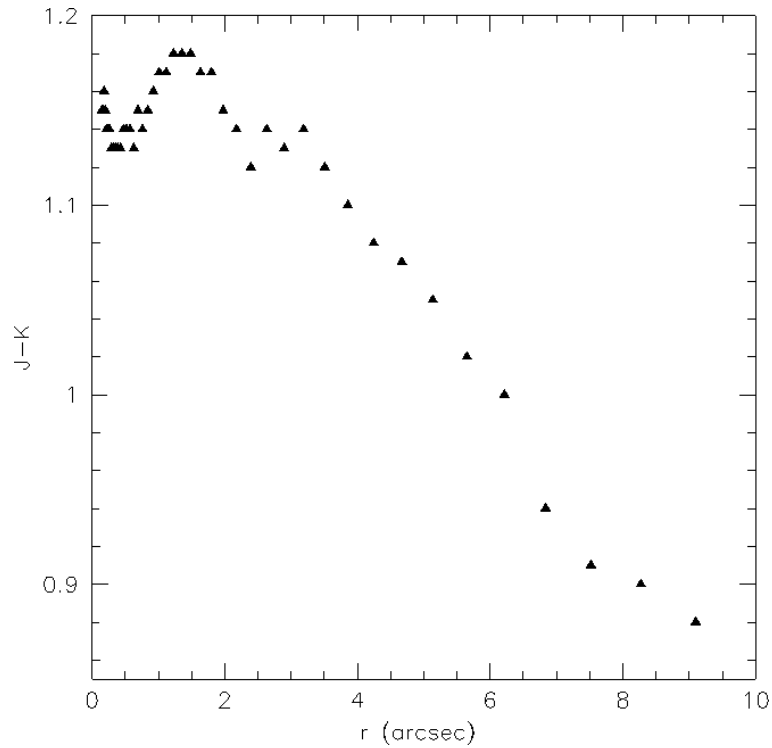


Figure 8. Mean J-K color profile. The error bar (± 0.04) is within the dimensions of data points.

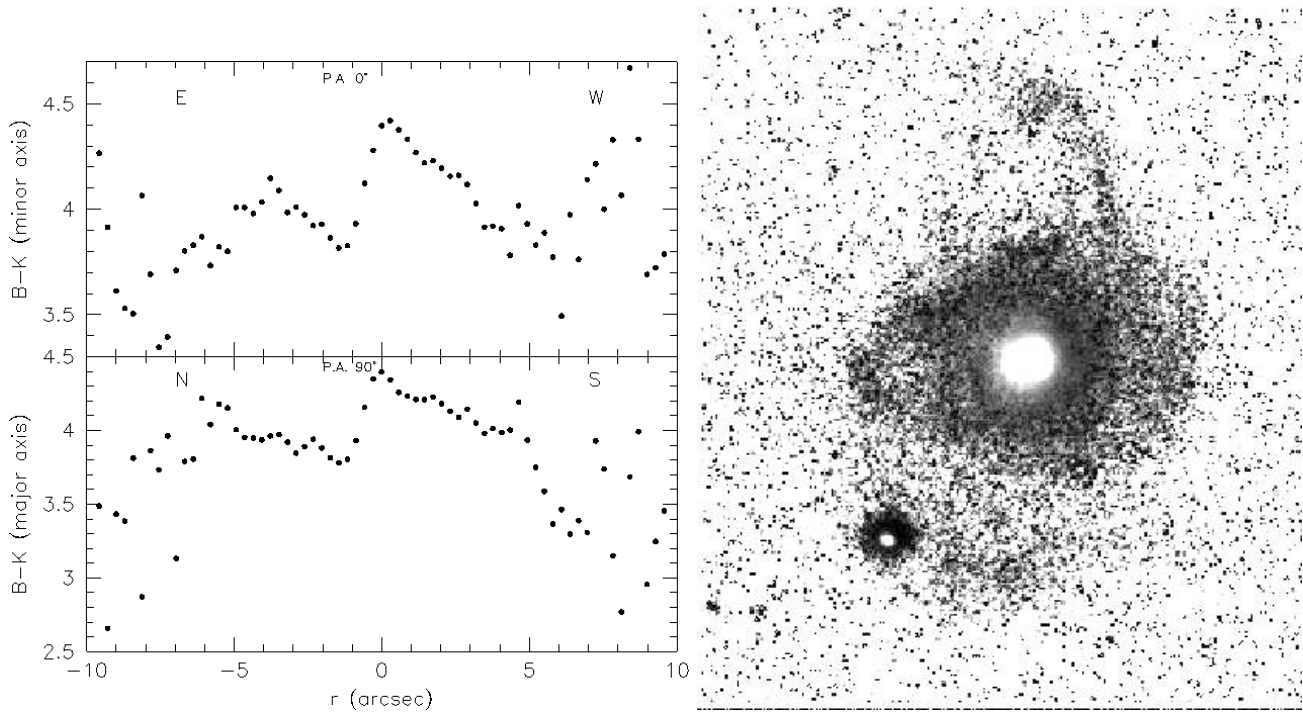


Figure 9. Left panel - B-K color profiles along the minor (top panel) and major (bottom panel) axis. The error bar (± 0.08) is within the dimensions of data points. Right panel - B-K color map. The North is up, while the east is on the left of the image. Lighter colors correspond to redder galaxy regions.

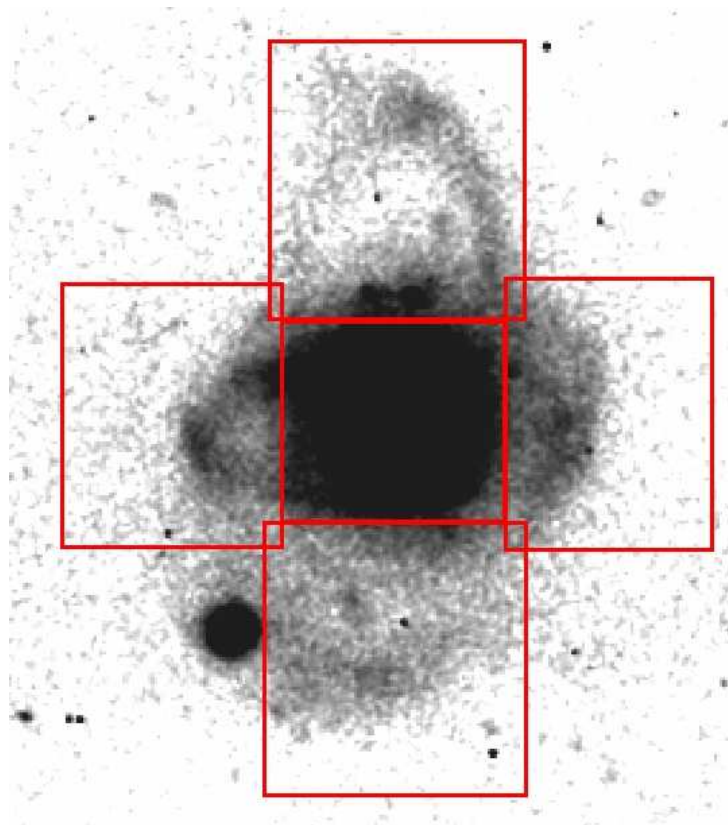


Figure 10. B band image with superimposed the five rectangles limiting the different areas where the integrated magnitudes have been computed. The North is up, while the east is on the left of the image.

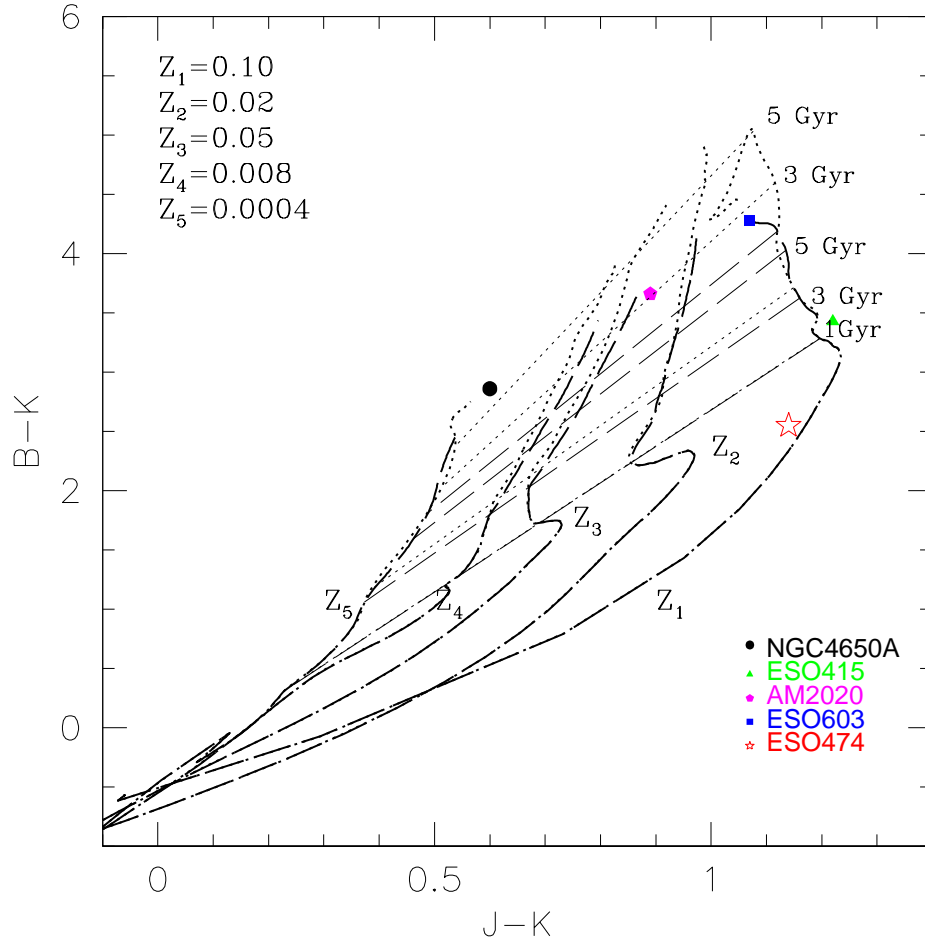


Figure 11. B-K vs J-K diagram of the evolutionary tracks for the stellar synthesis models optimized for the central component of ESO474-G26. We used models with a characteristic time scale $\tau = 1$ Gyr (heavy dotted lines) and models with $\tau = 7$ Gyrs (heavy dashed lines), computed for different metallicities as shown on the figure. Light dotted and and light dashed lines indicates loci of constant age for the different models; different ages are reported on the plot. The red star corresponds to the central object of ESO474-G26, while the other points correspond to the sample of PRGs in Iodice et al. (2002a,b).

Table 5. Galfit parameters.

Parameter	Value	Parameter	Value
<i>K band</i>		<i>B band</i>	
Component	Sersic	Component	Sersic
Integrated magnitude	11.30	Integrated magnitude	17.78
Effective radius	7 ± 0.01 arcsec	Effective radius	15.52 ± 0.05 arcsec
Sersic index	1.52 ± 0.01	Sersic index	3.13 ± 0.01
Axis ratio (b/a)	0.97 ± 0.01	Axis ratio (b/a)	0.99 ± 0.01
Position Angle	81.3 ± 1.7	Position Angle	101.0 ± 5.6

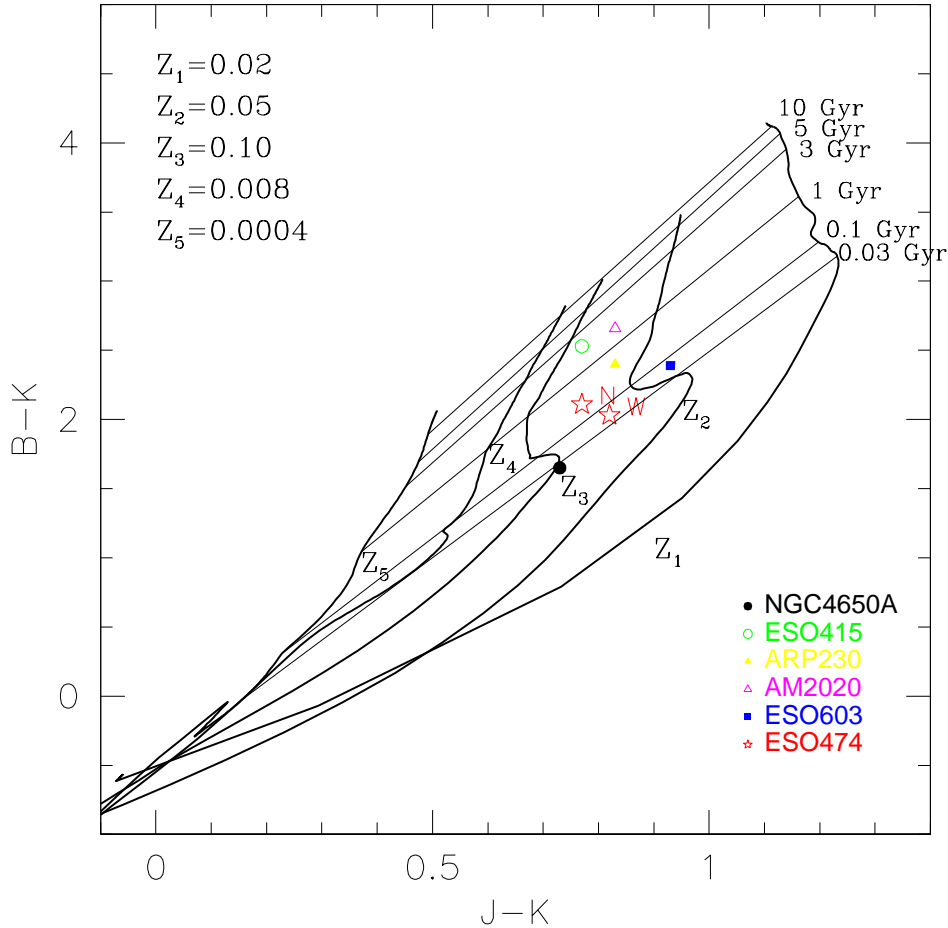


Figure 12. B-K vs J-K diagram of the evolutionary tracks for the stellar synthesis models optimized for the central component of ESO474-G26. For the polar structures of ESO474-G26 we used models with constant SFR computed for different metallicities (heavy lines). Light lines are loci of constant age; different ages are quoted on the plot. Red stars correspond to different regions of the polar rings in ESO474-G26, while the other points correspond to the sample of PRGs in Iodice et al. (2002a,b).

(and references therein) i.e., collapsing triaxial systems composed of dark matter (DM) and gas with density distribution $\rho \propto r^{-1}$, in different proportions and different total masses. We then allowed a large set of galaxy encounters involving systems with a range of mass ratios from 1:1 to 1:10. In order to exploit a vast range of orbital parameters, we carried out different simulations for each pair of interacting systems, varying the orbital initial conditions in order to have, for the ideal Keplerian orbit of two mass points, the first peri-center separation, p , ranging from the initial length of the major axis of the dark matter triaxial halo of the primary system to 1/10 of the same (major) axis.

For each of these separations, we changed the eccentricity in order to have hyperbolic orbits of different energies. For the most part we studied direct encounters, where the spins of the systems are equal (MC03), generally parallel to each other, and perpendicular to the orbital plane. However, we

also analyzed some cases with misaligned spins in order to enhance the effects of the system initial rotation on the results. Moreover, for a given set of encounters with the same orbital parameters we also examined the role of increasing initial gas fractions.

All simulations include self-gravity of gas, stars and DM, radiative cooling based on standard cooling function including metals, hydrodynamical pressure, shock heating, artificial viscosity, star formation (SF) and feedback from evolved stars and type II SNe, and chemical enrichment. The minimum temperature reached is 10^3 K to save time computing. Here, as in the following, cold gas is gas with temperature lower than 10^4 K, given that its cooling timescale is shorter than the snapshot time-range, as we will point out later on. The gravitational softening is taken to be 0.5 and 1 Kpc respectively for the gas and DM particles. The Initial Mass Function (IMF) is of Salpeter's type with upper mass limit

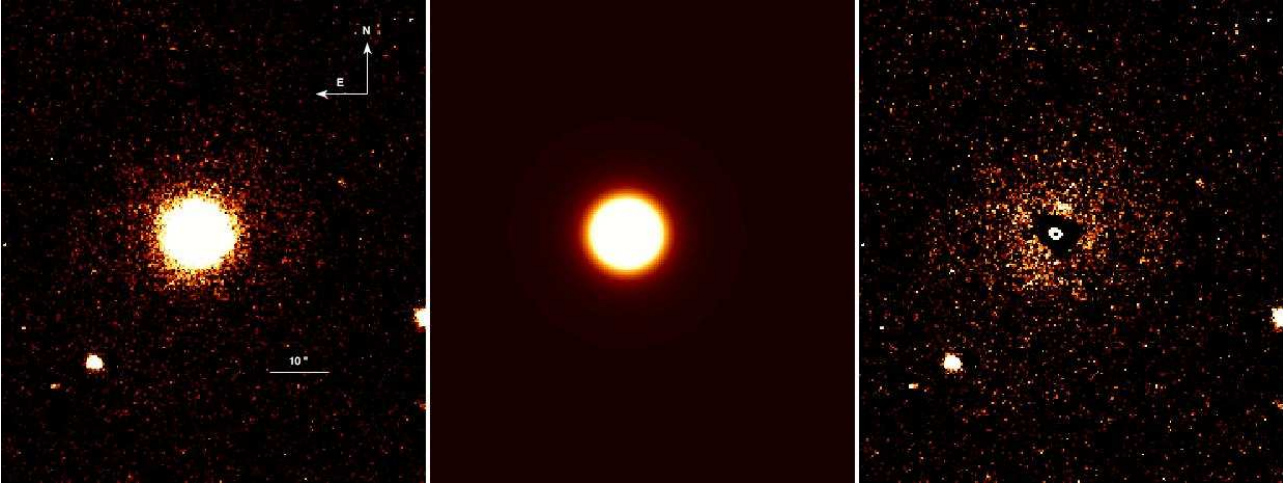


Figure 13. 2D fit of ESO474-G26. Left panel - K band image of ESO474-G26. Middle panel - K band model of the galaxy. Right panel - Residual of the subtraction of the model to the K band image.



Figure 14. 2D fit of ESO474-G26. Left panel - B band image of ESO474-G26. Middle panel - B band model of the galaxy. Right panel - Residual of the subtraction of the model to the B band image.

of $100 M_{\odot}$ and lower mass limit of $0.01 M_{\odot}$ (Salpeter 1955; see MC03 and references therein for a discussion). All our simulations provide the synthetic SED at each evolutionary step. The SED accounts for chemical evolution, stellar emission, internal extinction and re-emission by dust in a self-consistent way, as described in Spavone et al. (2009) and references therein, and extends over almost four orders of magnitude in wavelength, i.e., from 0.05 to $1000 \mu\text{m}$. So, each simulation self-consistently accounts for morphological, dynamical and chemo-photometric evolution.

The whole SED of ESO 474-G26 and its global properties are well matched by a major merger, i.e. with a 1:1 mass ratio. The total initial mass of the systems is $4 \times 10^{12} M_{\odot}$ with gas fraction 0.10, so that the total initial mass of the gas is $4 \times 10^{11} M_{\odot}$. The mass particle resolution is $1.33 \times 10^7 M_{\odot}$ for gas and $1.2 \times 10^8 M_{\odot}$ for DM particles. This requires 60000 initial particles.

The first pericenter separation, 101.4 Kpc, corresponds to 1/10 of the major axis of their halo; the orbit eccentricity is 1.3 and the anomaly corresponds to 200 degrees. The initial

haloes have perpendicular spins ($\lambda = 0.058$) and triaxiality ratio 0.84 (Mazzei & Curir 2003). Stars are born in the inner regions of their halos after about 2.5 Gyr from the beginning. Galaxies grow changing their shapes step by step as their trajectories are approaching and their halos mixing.

6.1 Evolution of ESO 474-G26

We match the global properties of ESO 474-G26 during a very active phase, due to the strong interaction between the systems, i.e. 11.2 Gyrs from the beginning of the simulation. The older stellar populations are 8.5 Gyr old, however the large majority of star clusters are younger than 6.5 Gyr. By averaging population ages inside $\sim r_{\text{eff}}(B)$ and $\sim 4r_{\text{eff}}(B)$, our fit corresponds respectively to a galaxy age of 2 Gyr and 4 Gyr. The B band absolute magnitude of the model, -22.31 mag, agrees well with the cosmologically corrected value from HyperLeda and the value in Table 1, as so as the K band absolute of the model, -25.32 (see Table 1). The mean velocity distribution along the galaxy major axis of

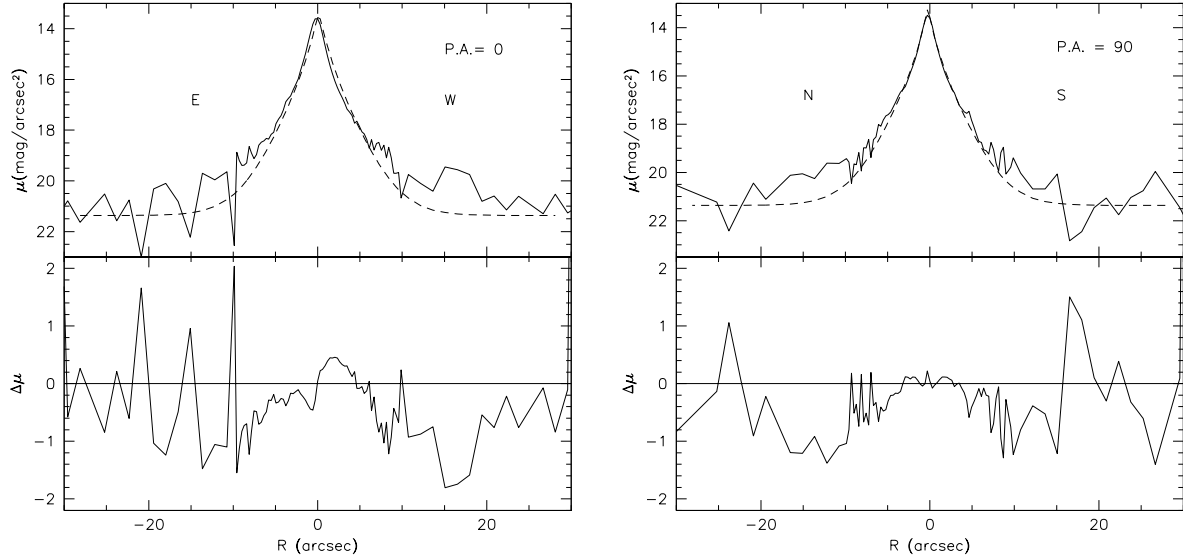


Figure 15. Top left panel-2-D fit of ESO474-G26 light distribution in the K band. The observed light profile along the minor axis (EW), is compared with those derived by the fit (dashed line). Bottom left panel - Residuals between the observed and the fitted light profiles. Top right panel-The same as above but for major axis (NS). Bottom right panel - Residuals between the observed and the fitted light profiles.

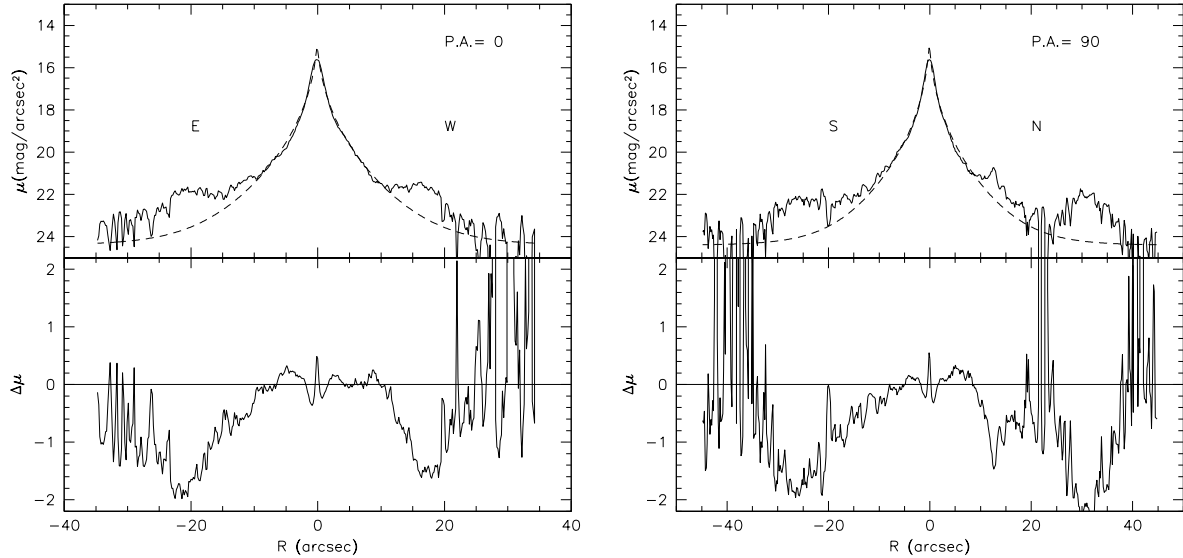


Figure 16. Top left panel-2-D fit of ESO474-G26 light distribution in the B band. The observed light profile along the minor axis (EW), is compared with those derived by the fit (dashed line). Bottom left panel - Residuals between the observed and the fitted light profiles. Top right panel-The same as above but for major axis (NS). Bottom right panel - Residuals between the observed and the fitted light profiles.

cold and warm gas, i.e. gas with temperature lower than 10^4 K whose cooling timescale is shorter than the snapshot time-range (38Myr), compares with the same distribution derived from $H\alpha$ measurements at the major axis position angles (P.A) of Whitmore et al. (1990), as shown in Figure 17; measurements in Whitmore et al. (1990) are corrected to account for a line of sight inclination angle of 52.2 degree (HyperLeda). Vertical dashed line corresponds to the inner

region ($R \leq 1$ Kpc) where model sampling could affect the results. We point out that the slightly difference, of almost 10 km/s, can be accounted for the error in the recession velocity of the galaxy (12 Km/s, by HyperLeda). At the selected snapshot the cold and warm gas, which will form new stars, is distributed in a ring (see Figure 18) surrounding the central spheroid.

Figure 19 shows the best fit of the predicted SED

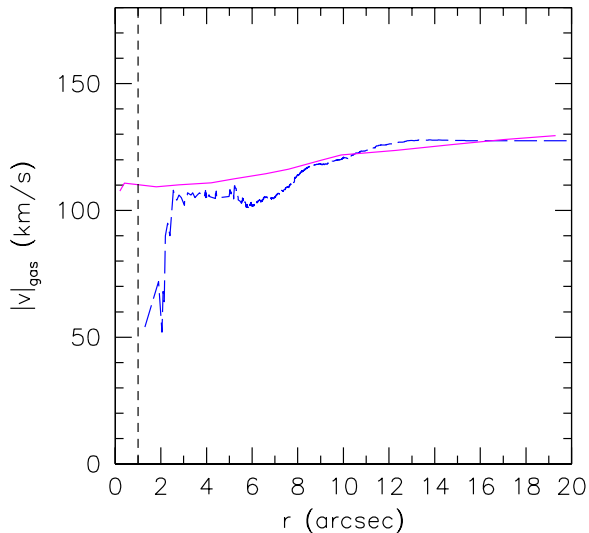


Figure 17. Blu dashed line shows the mean velocity distribution predicted for the cold and warm gas in our model (see text) along the galaxy major axis. Magenta solid line corresponds to the averaged velocity distribution as derived from H α measurements along the galaxy major axis, corrected for the inclination. Vertical dashed line corresponds to the inner region ($R \leq 1$ Kpc) where model sampling could affect the results.

by the simulation for ESO474-G26 to the available data. Dust components, warm and cold with PAH as discussed in Mazzei et al. (1992) with the same average properties as derived by Mazzei et al. (1994) and Mazzei & de Zotti (1994) for a complete sample of nearby early-type galaxies are included in the far-IR SED. The SFR inside $6 r_{eff}(B)$ (~ 60 Kpc) is $41 M_{\odot}/yr$, in agreement with radio estimates (see Sec. 1.2). The total mass inside $r_{eff}(B)$ is $1.30 \times 10^{11} M_{\odot}$ with 14.4% of dark matter, inside $2r_{eff}(B)$ raises to $3.50 \times 10^{11} M_{\odot}$ with 25% of DM and to $4.650 \times 10^{11} M_{\odot}$ with 44% of DM inside $4r_{eff}(B)$. The predicted M_{tot}/L_B ratio goes from $3 M_{\odot}/L_{\odot}$ at $r_{eff}(B)$ to $6.5 M_{\odot}/L_{\odot}$ at $4r_{eff}(B)$.

By inspecting the simulation at the snapshot corresponding to 0.5 Gyr after the merging (Figure 20), the remnant becomes smooth and the morphology resembles that of spheroidal early-type system.

7 DISCUSSION AND CONCLUSIONS

We have presented a detailed photometric study of the double ringed galaxy ESO474-G26, based on new NIR observations. The main results of the present work are: *i*) the central spheroidal component dominates the light in the NIR bands, particularly in the Ks band, while the rings emission becomes weaker from J to Ks bands; *ii*) by using the stellar population synthesis model (see sec. 5), the last burst of star formation is dated to be less than 1 Gyr for the central galaxy, and between 0.1 and 0.03 Gyr for the ring-like structures, comparable with those of other PRGs with nar-

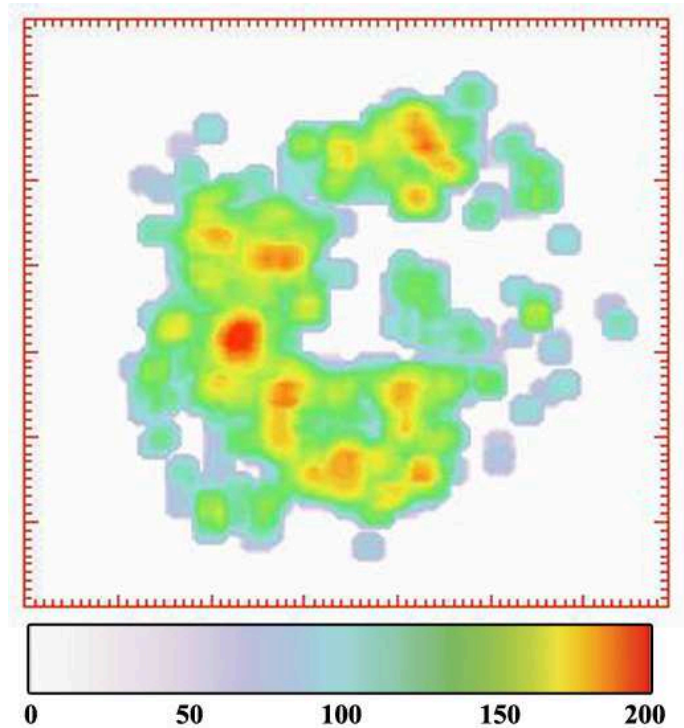


Figure 18. YZ map, 30 Kpc \times 30 Kpc, of cold and warm gas (see text) at the snapshot corresponding to the final merging stage (~ 9 Gyr). The mass of cold and warm gas is normalized to its total mass within the map; its density contrast is 200 with 60 equispaced levels and spatial resolution 0.4 Kpc.

row rings (see Figure 11 and 12); *iii*) the 2D model of the light distribution suggests that one of the two rings, most probably the polar one, extends till the galaxy center (see Figure 14); *iv*) the SED turns to be well matched by a major merger (see Figure 19).

The main goal of the analysis presented in this work is to address the most reliable formation scenario for ESO474-G26, by reconciling the observed properties for this peculiar object with those predicted by different formation mechanisms for such kind of systems. As widely discussed into sec. 1, the up-to-date scenarios proposed for PRGs formation are (1) the disruption of a dwarf companion galaxy orbiting around an early-type system, or the tidal accretion of gas stripping from a disk galaxy outskirts, (2) a dissipative merging of two disk galaxies, (3) accretion of cold gas from cosmic web filaments. In the case of ESO474-G26, we expect that the most likely formation scenario has to account for *i*) the morphology, i.e. the presence of two orthogonal ring-like structures around an almost spherical early-type object, *ii*) the observed colors and ages for both components, i.e. a good fit for the observed SED; *iii*) the observed kinematics; *iv*) the gas content and distribution. To this aim, we used the infrared photometry which has the main advantages to be less affected by dust absorption so it well traces the older stellar population.

In order to reproduce the structure of ESO474-G26, Reshetnikov et al. (2005) have performed N-body simulations of a low-velocity head-on collision between two galaxies with orthogonal spiral disks. In their simulations, the main galaxy was a giant spiral galaxy with a low gas fraction,

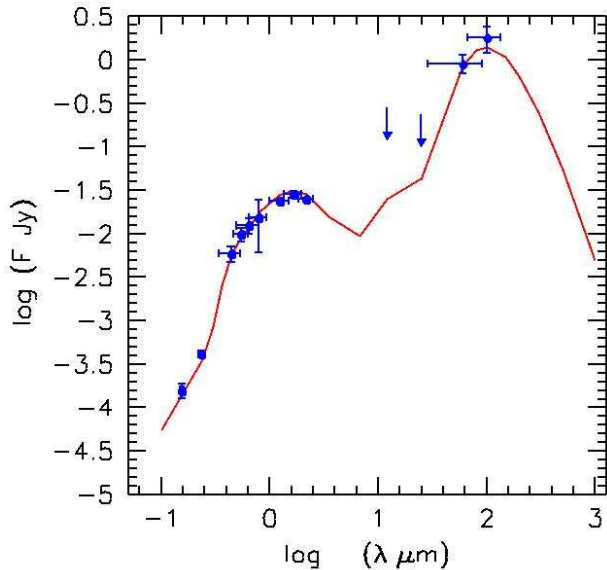


Figure 19. Continuous line (red) show the prediction of our model (see text). (Blue) filled circles correspond to data from NED and from Table 1. Arrows show upper limits; error bars account for band width and 3σ uncertainties. Dust components (warm and cold with PAH as discussed in Mazzei et al. (1992) with the same average properties as derived by Mazzei & de Zotti (1994) for a complete sample of nearby early-type galaxies are included (i.e. $I_0=46I_{local}$, $I_w=110I_{local}$, $R_{wc}=0.27$ and $r_d=30r_c$, as in Mazzei et al. 1994)

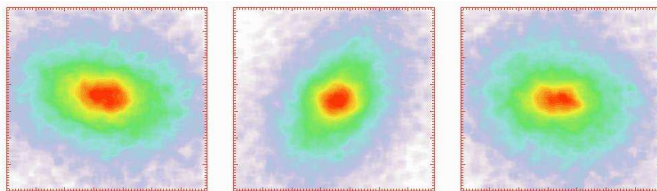


Figure 20. B band intrinsic flux map, $60\text{Kpc} \times 60\text{Kpc}$, of XY, YZ, and XZ projections at the snapshot corresponding to 0.5 Gyr after the merging. The remnant becomes smooth and the morphology resembles that of spheroidal early-type system. Each panel is normalized to its total flux; the density contrast is 200 with 60 equispaced levels, the spatial resolution 1.2 Kpc. The color scale is the same as in Fig. 18.

while the second galaxy was less massive but with a higher gas content. They found that, 350 Myr after the first crossing, the merger remnant shows an equatorial ring made up of stars coming from the intruder galaxy, and an expanding collisional polar ring. They found that the polar ring is a transient feature and that 1 Gyr after the full merging, the remnant becomes an elliptical-like object.

On the basis of these previous results and by taking into account the new NIR photometry, we have developed new SPH simulations of galaxy formation and evolution (Sect.6), in order to test the major merger scenario for ESO474-G26.

Differently from Reshetnikov et al. (2005), in our simulations no galaxies exist at the beginning, but only collapsing triaxial halos composed of dark matter and gas, in equal proportions in both the systems, with equal total masses (1:1) and perpendicular spins (Sect.6 for details). In the paper of Reshetnikov et al. (2005) galaxies with mass ratio 2.5:1 are separated by 70 Kpc and their relative velocity was 70 km/s whereas, in our case, the initial relative velocity of their centre of mass is $\simeq 104\text{Km/s}$ and its position corresponds to 233 Kpc in the XY, orbital plane. The total initial mass in Reshetnikov et al. (2005) is $8.8 \times 10^{11} M_\odot$, while in our simulation it is 4.5 times more. We confirm that a major merger of two haloes with a 1:1 mass ratio is able to well reproduce the observed structure and the properties of ESO474-G26: in particular, *i*) an excellent fit of the SED (see Figure 19), which is well-constrained by the NIR fluxes; by inspecting the simulation at the snapshot corresponding to 0.5 Gyr after the merging, *ii*) the remnant becomes smooth, the ring-like structure vanishes and the morphology resembles that of spheroidal early-type system (see Figure 20); *iii*) the predicted gas kinematics is consistent with the observed one along the galaxy major axis (see Figure 17); *iii*) the cold gas, which will form new stars, is distributed in a ring (see Figure 18) surrounding the central spheroid. As already pointed out by Reshetnikov et al. (2005), also this new simulation suggests that the structure of ESO474-G26 could be a transient phase and not a stable dynamical configuration.

In order to complete our analysis on the evolution history of ESO474-G26, we now examine if the other possible formation scenarios, could also equally well match its observed properties.

The tidal accretion scenario, in which gas is stripped from a gas-rich donor in a particular orbital configuration (Bournaud & Combes 2003), is able to produce wide rings and/or disks both around a disk or an elliptical galaxy: in this framework, in the field around the new forming ring galaxy the gas-rich donor galaxy is still present. In the case of ESO474-G26, inside a radius of about five times its diameter, as suggested by Brocca et al. (1997), there are no close companions as possible donor galaxy candidates. Moreover, in the tidal accretion scenario, the total amount of accreted gas by the early-type object is about 10% of the gas in the disk donor galaxy, i.e. up to $10^9 M_\odot$: the high baryonic mass (star plus gas) in the rings of ESO474-G26, which is about $10^{10} M_\odot$, turns to be not consistent with this limit and further confirms that the tidal accretion need to be ruled out. The gradual disruption of a dwarf satellite galaxy cannot reconcile with a multiple ring structure.

Finally, the cold accretion scenario predict the formation of wide disk-like structures around an host galaxy. In this scenario, a long-lived polar structure may form through cold gas accretion along a filament extended for $\sim 1\text{Mpc}$ into the virialized dark matter halo (Macciò et al. 2006). In this formation scenario, there are no limits to the mass of the accreted material, thus, a very massive polar disk may develop either around a stellar disk or a spheroid. Brook et al. (2008), by using high-resolution cosmological simulations of galaxy formation, have confirmed and strengthened the formation scenario proposed by Macciò et al. (2006). However, Brook et al. (2008) in their study have referred to objects characterized by polar structures with disk galaxy charac-

teristics. In other galaxies, such as ESO474-G26, the polar structure is better described as a ring, with gas and stars in a narrow annulus. For this reason, the study of Brook et al. (2008) is not conclusive on this issue, and the classic merging and accretion models remain viable explanations for the formation of narrow polar ring structures. Spavone et al. (2011), by studying the formation mechanism of the PRG UGC7576, were able to test and confirm the cold accretion for this object, whose polar structure is a ring rather than a disk. However, differently from ESO474-G26, UGC7576 have a wide ring-like structure. Moreover, the narrow rings observed in ESO474-G26 are very faint structures, and they are not able to survive to the repeated accretion and mergers predicted by Brook et al. (2008).

We can thus conclude that the major merger is the most plausible scenario for the formation of the complex double ringed structure of ESO474-G26.

ACKNOWLEDGEMENTS

The authors thank the referee, Frederic Bournaud, for the detailed and constructive report, which allowed them to improve the paper. E.I. wish to thank E. Pompei for the support given during the data acquisition. This work is based on observations made with ESO Telescopes at the Paranal Observatories under programme ID < 70.B - 0253(A) > and < 74.B - 0626(A) >. We acknowledge financial contribution from the agreement ASI-INAF I/009/10/0 and M.S. acknowledges financial support from the “Fondi di Ateneo 2011” (ex 60 %) of Padua University. V.R. acknowledges partial financial support from the RFBR grant 11 – 02 – 00471–a.

REFERENCES

- Arnaboldi M., Oosterloo T., Combes F., Freeman K. C., Koribalski B., 1997, *AJ*, 113, 585
 Bekki K., 1998a, *ApJ*, 499, 635
 Bekki K., 1998b, *ApJL*, 502, L133+
 Bertola F., Galletta G., Zeilinger W. W., 1985, *ApJL*, 292, L51
 Bothun G. D., Gregg M. D., 1990, *ApJ*, 350, 73
 Bournaud F., Combes F., 2003, *A&A*, 401, 817
 Bournaud F., Jog C. J., Combes F., 2005, *A&A*, 437, 69
 Brocca C., Bettoni D., Galletta G., 1997, *A&A*, 326, 907
 Brook C. B., Governato F., Quinn T., Wadsley J., Brooks A. M., Willman B., Stilp A., Jonsson P., 2008, *ApJ*, 689, 678
 Bruzual G., Charlot S., 2003, *MNRAS*, 344, 1000
 Cole S., Lacey C. G., Baugh C. M., Frenk C. S., 2000, *MNRAS*, 319, 168
 Condon J. J., Cotton W. D., Greisen E. W., Yin Q. F., Perley R. A., Taylor G. B., Broderick J. J., 1998, *AJ*, 115, 1693
 Conselice C. J., Bershadsky M. A., Dickinson M., Papovich C., 2003, *AJ*, 126, 1183
 Emsellem E., Cappellari M., Krajnović D. e. a., 2011, *MNRAS*, 414, 888
 Gallagher J. S., Sparke L. S., Matthews L. D., Frattare L. M., English J., Kinney A. L., Iodice E., Arnaboldi M., 2002, *ApJ*, 568, 199
 Galletta G., Sage L. J., Sparke L. S., 1997, *MNRAS*, 284, 773
 Graham J. A., 1982, *PASP*, 94, 244
 Hancock M., Smith B. J., Struck C., Giroux M. L., Hurlock S., 2009, *AJ*, 137, 4643
 Hopkins A. M., Miller C. J., Nichol R. C., Connolly A. J., Bernardi M., Gómez P. L., Goto T., Tremonti C. A., Brinkmann J., Ivezić Ž., Lamb D. Q., 2003, *ApJ*, 599, 971
 Iodice E., Arnaboldi M., De Lucia G., Gallagher III J. S., Sparke L. S., Freeman K. C., 2002, *AJ*, 123, 195
 Iodice E., Arnaboldi M., Saglia R. P., Sparke L. S., Gerhard O., Gallagher J. S., Combes F., Bournaud F., Capaccioli M., Freeman K. C., 2006, *ApJ*, 643, 200
 Iodice E., Arnaboldi M., Sparke L. S., Freeman K. C., 2002, *A&A*, 391, 117
 Iodice E., Arnaboldi M., Sparke L. S., Gallagher J. S., Freeman K. C., 2002, *A&A*, 391, 103
 Khochfar S., Emsellem E., Serra e. a., 2011, *MNRAS*, 417, 845
 Landolt A. U., 1983, *AJ*, 88, 439
 Macciò A. V., Moore B., Stadel J., 2006, *ApJL*, 636, L25
 Mazzei P., 2003, *MemSAIt*, 74, 498
 Mazzei P., Curir A., 2003, *ApJ*, 591, 784
 Mazzei P., de Zotti G., 1994, *ApJ*, 426, 97
 Mazzei P., de Zotti G., Xu C., 1994, *ApJ*, 422, 81
 Mazzei P., Xu C., de Zotti G., 1992, *A&A*, 256, 45
 Moiseev A. V., Smirnova K. I., Smirnova A. A., Reshetnikov V. P., 2011, *MNRAS*, 418, 244
 Peng C. Y., Ho L. C., Impey C. D., Rix H.-W., 2002, *AJ*, 124, 266
 Persson S. E., Murphy D. C., Krzemiński W., Roth M., Rieke M. J., 1998, *AJ*, 116, 2475
 Reshetnikov V., Bournaud F., Combes F., Faúndez-Abans M., de Oliveira-Abans M., van Driel W., Schneider S. E., 2005, *A&A*, 431, 503
 Reshetnikov V., Sotnikova N., 1997, *A&A*, 325, 933
 Reshetnikov V. P., Hagen-Thorn V. A., Yakovleva V. A., 1994, *A&A*, 290, 693
 Reshetnikov V. P., Hagen-Thorn V. A., Yakovleva V. A., 1995, *A&A*, 303, 398
 Rossa J., Laine S., van der Marel R. P., Mihos J. C., Hibbard J. E., Böker T., Zabludoff A. I., 2007, *AJ*, 134, 2124
 Salpeter E. E., 1955, *ApJ*, 121, 161
 Schweizer F., Whitmore B. C., Rubin V. C., 1983, *AJ*, 88, 909
 Sersic J. L., 1968, *Atlas de galaxias australes. Cordoba, Argentina: Observatorio Astronomico*, 1968
 Spavone M., Iodice E., Arnaboldi M., Gerhard O., Saglia R., Longo G., 2010, *ApJ*, 714, 1081
 Spavone M., Iodice E., Arnaboldi M., Longo G., Gerhard O., 2011, *A&A*, 531, A21
 Spavone M., Iodice E., Calvi R., Bettoni D., Galletta G., Longo G., Mazzei P., Minervini G., 2009, *MNRAS*, 393, 317
 Swaters R. A., Rubin V. C., 2003, *ApJL*, 587, L23
 Tal T., van Dokkum P. G., Nelan J., Bezanson R., 2009, *AJ*, 138, 1417
 Whitmore B. C., Lucas R. A., McElroy D. B., Steiman-

Cameron T. Y., Sackett P. D., Olling R. P., 1990, AJ,
100, 1489

This paper has been typeset from a \TeX / \LaTeX file prepared
by the author.